

Title here

Elio Campitelli * and Leandro Díaz

CIMA UBA blablabla

Carolina Vera

⁵ **Corresponding author:* Elio Campitelli, elio.campitelli@cima.fcen.uba.ar

ABSTRACT

Enter the text of your abstract here. This is a sample American Meteorological Society (AMS) \LaTeX template. This document provides authors with instructions on the use of the AMS \LaTeX template. Authors should refer to the file `amspaper.tex` to review the actual \LaTeX code used to create this document. The `template.tex` file should be modified by authors for their own manuscript.

10 *Significance statement.* This is significant because I wrote it.

11 **1. Introduction**

12 yada yada SAM yada yada circulation.. yada yada so important. yada yada many impacts.

13 **2. Methods**

14 **1) DATA**

15 We used monthly geopotential height at 2.5 longitude by 2.5 latitude resolution from ERA5
16 (Hersbach et al.) for the period 1979 to 2018 (inclusive).

17 Monthly temperature NOAA Global Surface Temperature (NOAAGlobalTemp) 5.0 degree lati-
18 tude x 5.0 degree longitude global grid (Vose et al. 2012; Smith et al. 2008). The same analysis
19 was carried out using CRUTEM4 (Osborn and Jones 2014) (not shown).

20 We used monthly precipitation data from CPC Merged Analysis of Precipitation (Xie and Arkin
21 1997) 2.5 degree latitude x 2.5 degree longitude.

22 **2) DEFINITION OF INDICES**

23 We defined the Southern Annular Mode (SAM) as the leading EOF of the monthly anomalies of
24 geopotential field at 700 hPa south of 20°S (citation?). The EOF was performed by computing the
25 Singular Value Decomposition of the data matrix consisting in 481 rows and 4176 columns (144
26 points of longitude and 29 points of latitude). The values were weighted by the square root of the
27 cosine of latitude to account for the non-equal area of each gridpoint (Chung and Nigam 1999).
28 This same method was used at the rest of the levels considered in this paper.

29 To separate between the zonally symmetric and asymmetric components of the SAM, we com-
30 puted the zonal mean and anomalies of the full SAM spatial pattern. The results are shown in

31 Figure 5 for 700hPa. The full spatial signal ($\text{EOF}_1(\lambda, \phi)$) is the sum of the zonally asymmetric
32 ($\text{EOF}_1^*(\lambda, \phi)$) and symmetric ($[\text{EOF}_1](\lambda, \phi)$) components. We then compute the “Full”, “Asym-
33 metric” and “Symmetric” indices, by regressing each geopotential field on these patterns (weighting
34 by the cosine of latitude).

35 The three indices are normalised by dividing them by the standard deviation of the “Full” index
36 at each level. This means that comparing the magnitude between indices is meaningful, but it also
37 means that not every index will have unit standard deviation.

38 3) SIGNIFICANCE

39 We adjusted p-values for False Detection Rate following Wilks (2016).

40 3. Results

41 a. Temporal evolution

42 Figure 6 shows the resulting Asymmetric and Symmetric time series corresponding to 700 and
43 30hPa. blablababla

- 44 • stratosphere clearly nor normally distributed. a lot of values near 0 and some relatively high
45 outliers. Especially true int he case of the asymmetric index. High frequency variability.
- 46 • In both levels, there’s correlation between the series (expected),

47 Correlations between the Asymmetric and Symmetric series are rather constant throught the
48 troposphere, fluctuating between 0.39 and 0.45 (Figure 7). Futhermore, the cross-correlation of
49 each series across levels –shown in Figure 8– are high in the trosposphere (greater than 0.9)
50 for both indices. This suggests that both the Asymmetric and the Symemtric component of
51 the tropospheric SAM are highly vertically coherent, both in their individual evolution and their

temporal relationship. This is to be expected since the SAM is mostly equivalent barotropic (citaaaa).

In the stratosphere the situation is different. As can be seen in Figure 7, the relationship between the Asymmetric and Symmetric indices varies with height above 100 hPa. It starts to decrease right over the tropopause, reaches a minimum of 0.21 at 20 hPa and then it increases again monotonically with height up to the uppermost level of the reanalysis. The cross-correlation across levels in the stratosphere is generally weaker than in the troposphere (Figure 8). Furthermore, above 100 hPa, the cross-correlation decreases more rapidly with height for the Symmetric SAM than for the Asymmetric SAM as evidenced by the wider dark red areas near the diagonal in Figure 8b) vs. Figure 8c). Moreover, the stratospheric Symmetric SAM seems to be slightly more connected to the troposphere than the Asymmetric SAM; this can be seen by the lower correlation values in the top right quadrant of Figure 8b) in comparison with Figure 8c).

Figure 8a) show the cross-correlation across levels for the Full SAM index.

b. Spatial patterns

To understand the spatial patterns associated with both indices we regressed monthly geopotential anomalies into both indices using multiple regression (Figure A6 illustrates the difference between computing two simple regressions and one multiple regression).

Figure 9 shows the spatial year-long regression for selected levels. In the troposphere the Full annular mode is clearly “contaminated” with well known zonal asymmetries (panels g and j) which are successfully separated by our methodology (panels h, i, k and l). In the stratosphere, the spatial pattern associated with the Full SAM is much more clearly dominated by a zonally symmetric, monopolar structure (panels a and d) that is, however, not perfectly centered in the south pole. The monopoles obtained by multiple regression with the Asymmetric and Symmetric SAM (panels c

75 and f in Figure 9) is much more symmetric and the shift from total symmetry is captured by the
76 regression pattern of the Asymmetric SAM as a wave-1 pattern (panels b and e).

77 The amplitude of each zonal wave number at each latitude at 50 hPa and 700 hPa is shown
78 in Figure 10, where wave number zero represents the zonal mean. Comparing between rows,
79 this Figure quantifies the relatively clean separation between the zonally symmetric and zonally
80 asymmetric structures, as its evident how the mixture of waves of the Full field (first row) is very
81 similar to the sum of the waves of the Asymmetric and Symmetric field (second and third row,
82 respectively). The second row of Figure 10 shows that the Asymmetric SAM is overwhelmingly
83 dominated by wave 1 in the stratosphere (panel b), while in the stratosphere it is composed of zonal
84 waves 3 to 1 in decreasing level of importance.

85 From Figure 9 it appears that the vertical structure of the Asymmetric SAM is equivalent
86 barotropic in the troposphere but baroclinic in the stratosphere. Anomalies are centered in the same
87 locations in the troposphere (panels h and k), but show westerly displacement in the stratosphere
88 (panels b and e). This is expanded in Figure 11, which shows a vertical cross-section of the regression
89 coefficient corresponding to the middle row of Figure 9, area-weighted averaged between 65 and
90 40 degrees South. Below 100 hPa, anomalies are completely vertical, while above they show an
91 important westerly tilt with height.

98 1) IMPACTS

103 *Acknowledgments.* CMAP Precipitation data provided by the NOAA/OAR/ESRL PSL, Boulder,
104 Colorado, USA, from their Web site at <https://psl.noaa.gov/>

105 NOAA Global Surface Temperature (NOAAGlobalTemp) data provided by the
106 NOAA/OAR/ESRL PSL, Boulder, Colorado, USA, from their Web site at <https://psl.noaa.gov/>

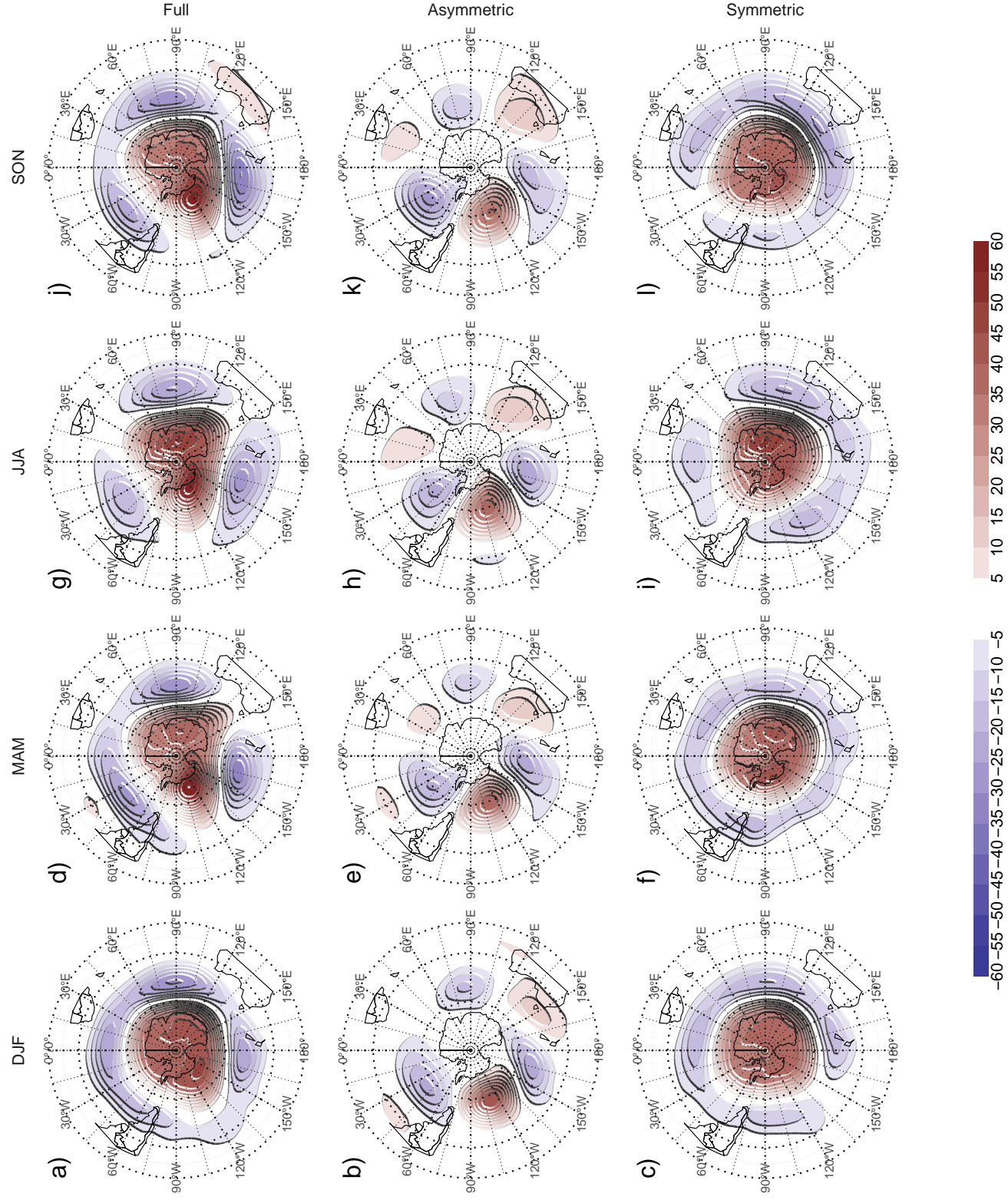


Fig. 1. Seasonal regression patterns of geopotential height at 700 hPa with the Full, Asymmetric and Symmetric SAM. The regression patterns for Asymmetric and Symmetric SAM are the result of one multiple regression using both indices, not of two simple regressions involving each index by

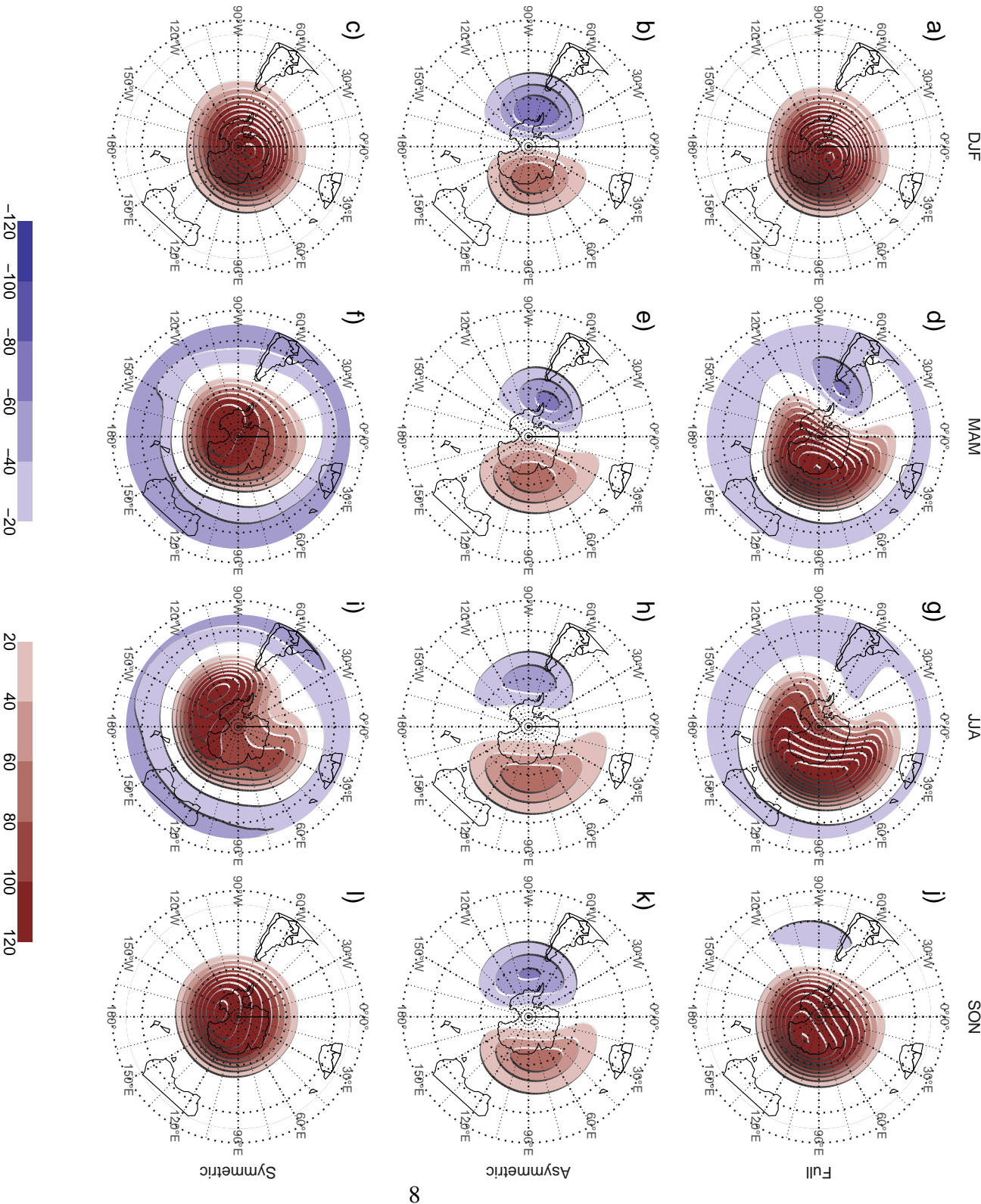


Fig. 2. Seasonal regression patterns of geopotential height at 30 hPa with the Full, Asymmetric and Symmetric SAM. The regression patterns for Asymmetric and Symmetric SAM are the result of one multiple regression using both indices, not of two simple regressions involving each index by itself.

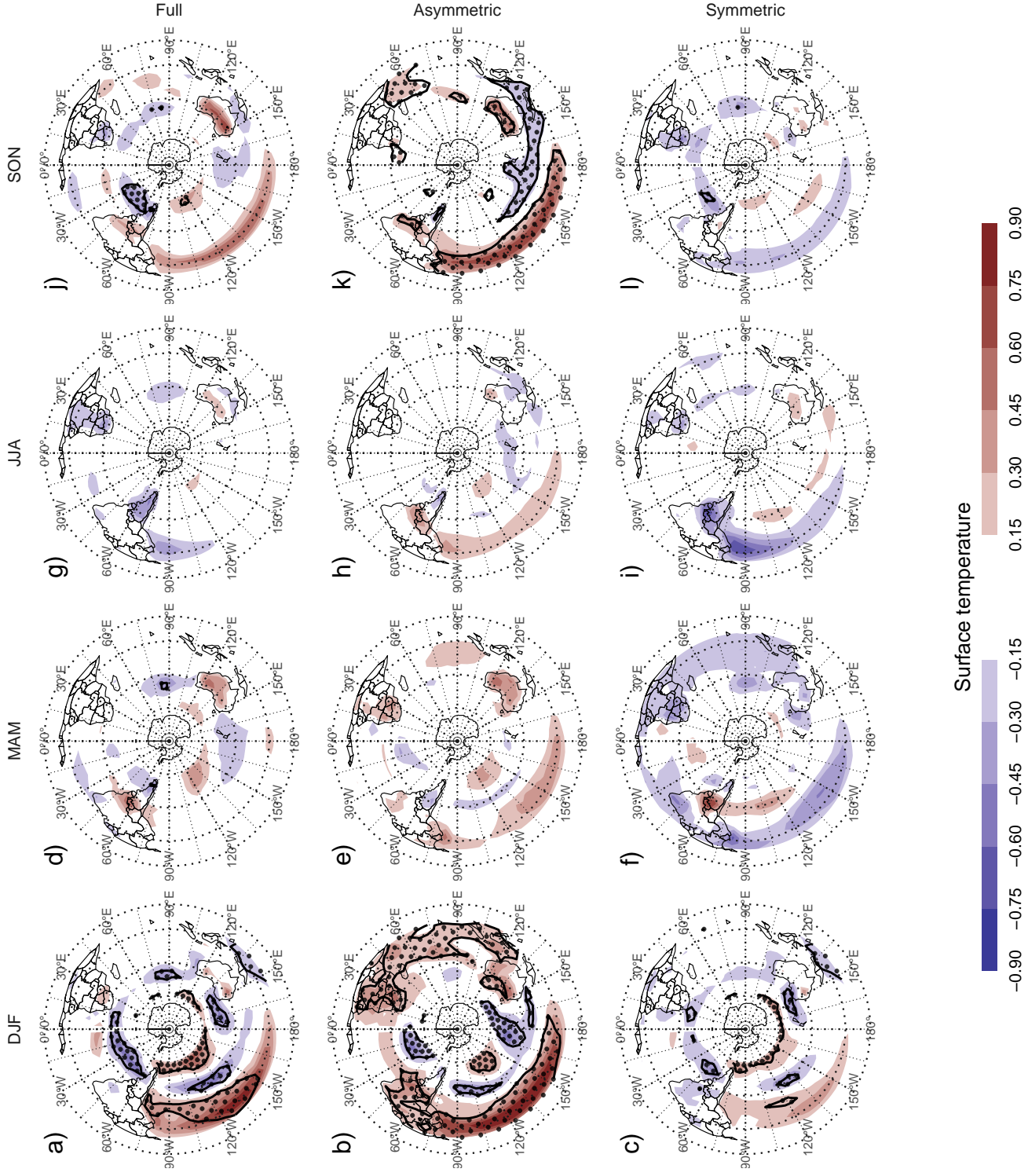


Fig. 3. Regression pattern of surface temperature with Asymmetric and Symmetric SAM. P-values smaller than 0.05 (controlling for False Detection Rate) as hatched areas.

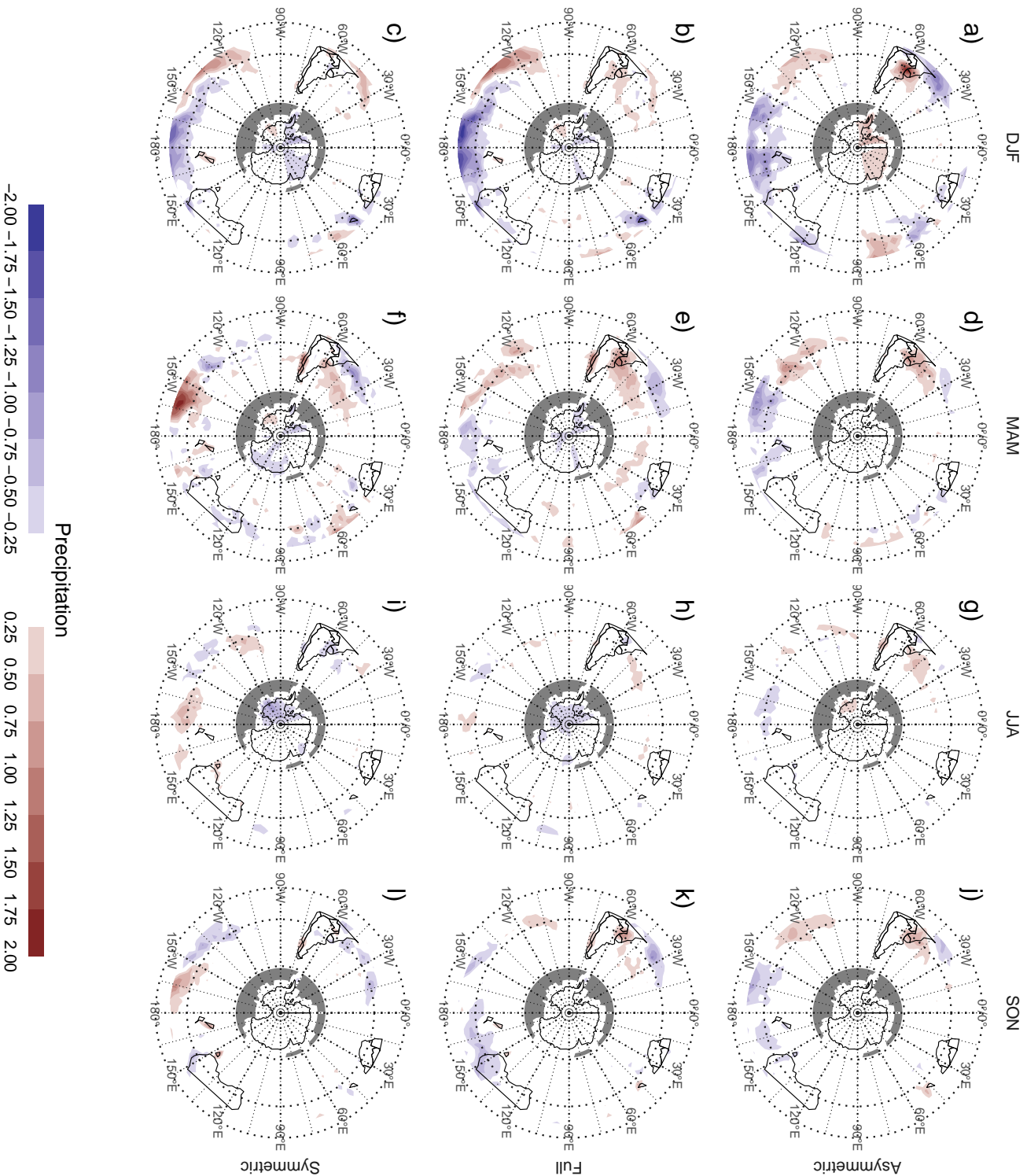


FIG. 4. Regression pattern of precipitation with Asymmetric and Symmetric SAM. P-values smaller than 0.05 (controlling for False Detection Rate) as hatched areas.

References

- Chung, C., and S. Nigam, 1999: Weighting of geophysical data in Principal Component Analysis. *Journal of Geophysical Research: Atmospheres*, **104 (D14)**, 16 925–16 928, doi: 10.1029/1999JD900234.
- Hersbach, H., and Coauthors, 2015: The ERA5 global reanalysis. *Quarterly Journal of the Royal Meteorological Society*, **n/a (n/a)**, doi:10.1002/qj.3803.
- Osborn, T. J., and P. D. Jones, 2014: The CRUTEM4 land-surface air temperature data set: Construction, previous versions and dissemination via Google Earth. *Earth System Science Data*, **6 (1)**, 61–68, doi:10.5194/essd-6-61-2014.
- Smith, T. M., R. W. Reynolds, T. C. Peterson, and J. Lawrimore, 2008: Improvements to NOAA’s Historical Merged Land–Ocean Surface Temperature Analysis (1880–2006). *J. Climate*, **21 (10)**, 2283–2296, doi:10.1175/2007JCLI2100.1.
- Vose, R. S., and Coauthors, 2012: NOAA’s Merged Land–Ocean Surface Temperature Analysis. *Bull. Amer. Meteor. Soc.*, **93 (11)**, 1677–1685, doi:10.1175/BAMS-D-11-00241.1.
- Wilks, D. S., 2016: “The Stippling Shows Statistically Significant Grid Points”: How Research Results are Routinely Overstated and Overinterpreted, and What to Do about It. *Bull. Amer. Meteor. Soc.*, **97 (12)**, 2263–2273, doi:10.1175/BAMS-D-15-00267.1.
- Xie, P., and P. A. Arkin, 1997: Global Precipitation: A 17-Year Monthly Analysis Based on Gauge Observations, Satellite Estimates, and Numerical Model Outputs. *Bull. Amer. Meteor. Soc.*, **78 (11)**, 2539–2558, doi:10.1175/1520-0477(1997)078<2539:GPAYMA>2.0.CO;2.

APPENDIX

Extra figures

129	LIST OF FIGURES	
130	Fig. 1. Seasonal regression patterns of geopotential height at 700 hPa with the Full, Asymmetric	
131	and Symmetric SAM	7
132	Fig. 2. Seasonal regression patterns of geopotential height at 30 hPa with the Full, Asymmetric and	
133	Symmetric SAM	8
134	Fig. 3. Regression pattern of surface temperature with Asymmetric and Symmetric SAM	9
135	Fig. 4. Regression pattern of precipitation with Asymmetric and Symmetric SAM	10
136	Fig. 5. Spatial patterns of the first EOF of 700 hPa geopotential height	14
137	Fig. 6. Time series for the asymmetric SAM and symmetric SAM	15
138	Fig. 7. Correlation between the Symmetric and Asymmetric SAM at each level	16
139	Fig. 8. Cross correlation between levels of the Full, Asymmetric and Symmetric SAM	17
140	Fig. 9. Regression patterns of geopotential height at 30, 300 and 700 hPa with the Full, Asymmetric	
141	and Symmetric SAM	18
142	Fig. 10. Planetary wave amplitude for the regression patterns at 50 and 700 hPa	19
143	Fig. 11. Asymmetric coefficient of the multiple regression of mean monthly geopotential height	
144	anomalies between 65 and 40 South	20
145	Fig. A1. Lag-correlation between Symmetric and Asymmetric SAM at each level.	21
146	Fig. 12. Cross-correlation functions for each index and two different base levels	22
147	Fig. A2. Fourier spectrum of each timeseries. The shading indicates the 95% area derived by fitting	
148	an AR process to each series and bootstrapping 5000 simulated samples.	23
149	Fig. A3. Autocorrelation functions of each timeseries	24
150	Fig. A4. Trends for each index at each level. Shading indicates the 95% confidence interval.	25
151	Fig. A5. Regression pattern of precipitation with Asymmetric and Symmetric SAM. P-values smaller	
152	than 0.05 (controlling for False Detection Rate) as hatched areas.	26
153	Fig. A6. Regressions maps resulting from performing one multiple regression (a. and b.) and from	
154	performing two simple regressions (c. and d.)	27
155	Fig. 13.	28

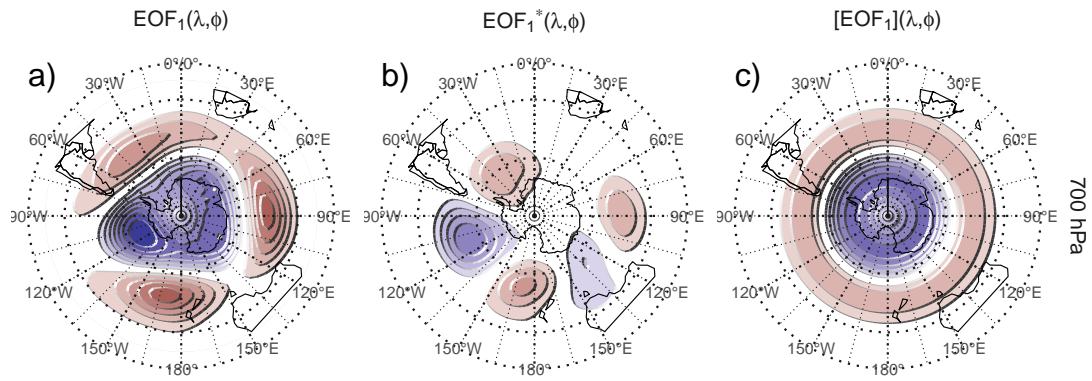


FIG. 5. Spatial patterns of the first EOF of 700 hPa geopotential height. Full field (left), zonally asymmetric component (middle) and zonally symmetric component (right). Arbitrary units.

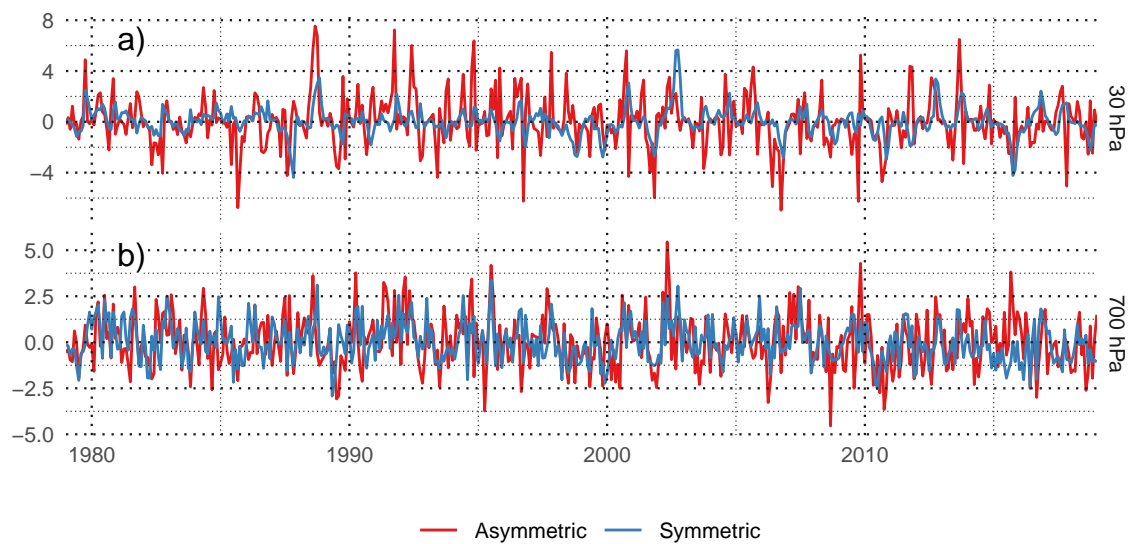


FIG. 6. Time series for the asymmetric SAM and symmetric SAM.

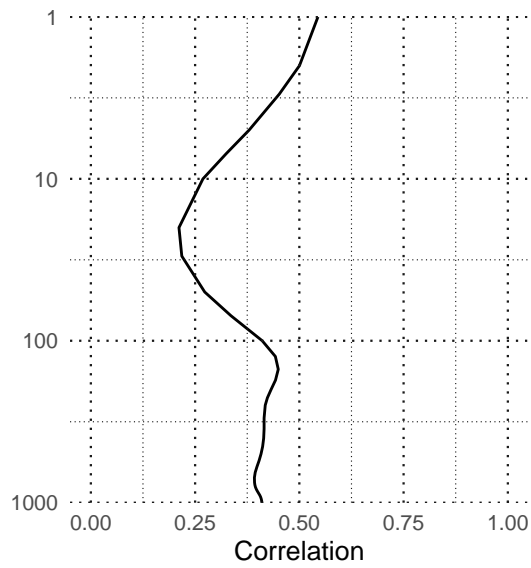


FIG. 7. Correlation between the Symmetric and Asymmetric SAM at each level.

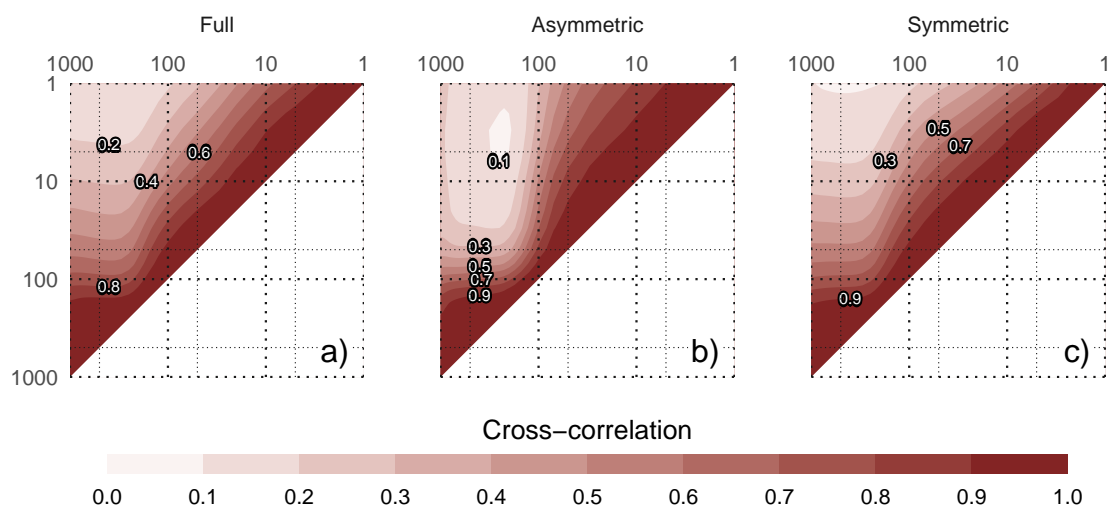


FIG. 8. Cross correlation between levels of the Full, Asymmetric and Symmetric SAM.

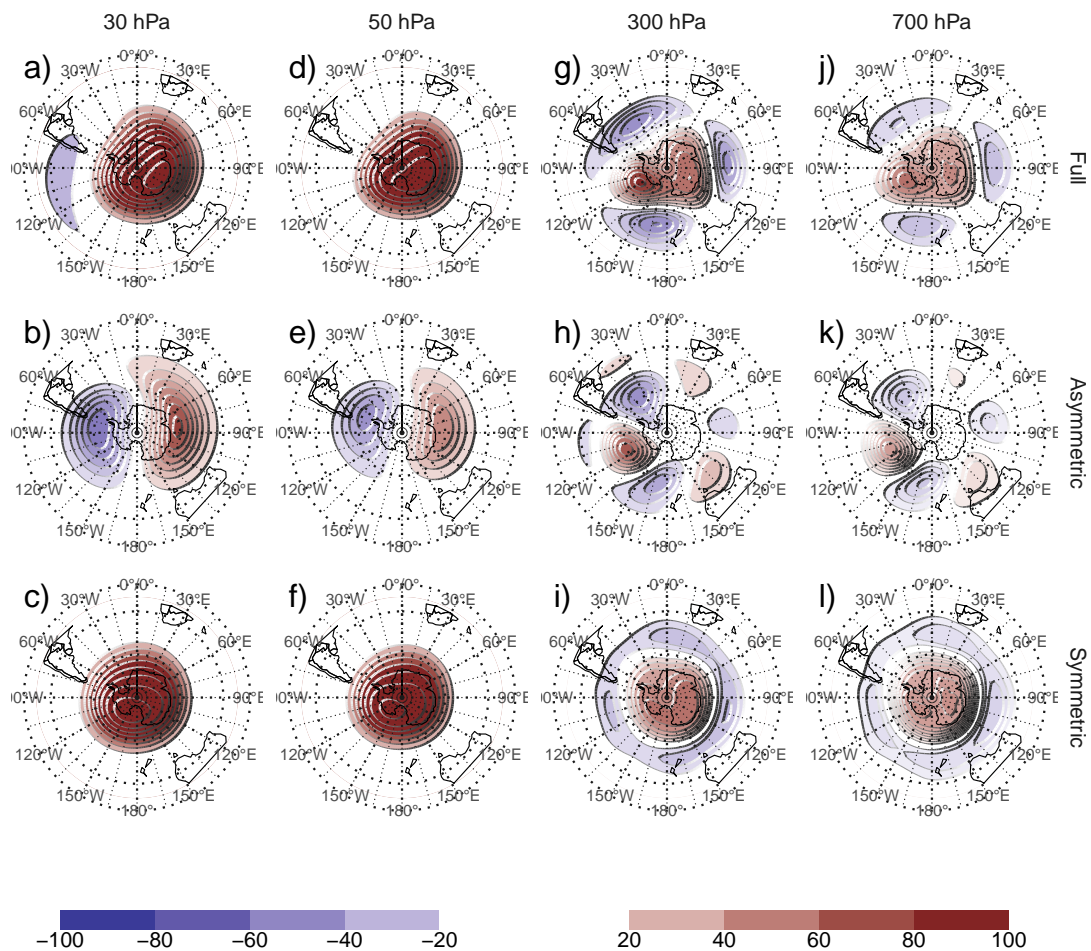


FIG. 9. Regression patterns of geopotential height at 30, 300 and 700 hPa with the Full, Asymmetric and Symmetric SAM. The regression patterns for Asymmetric and Symmetric SAM are the result of one multiple regression using both indices, not of two simple regressions involving each index by itself.

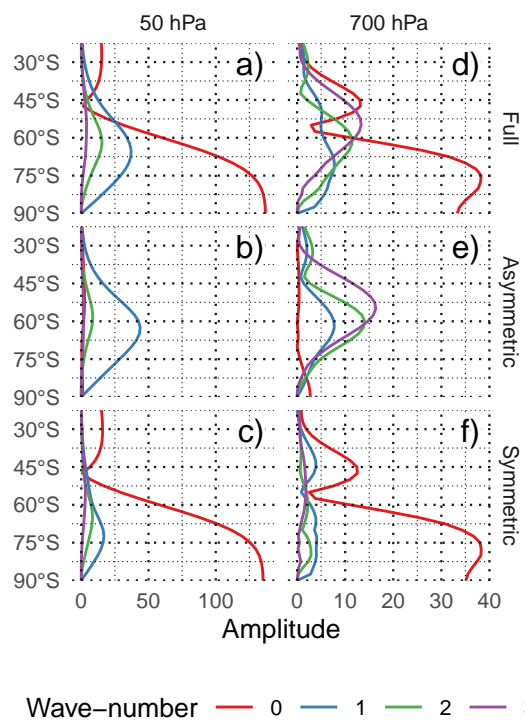


FIG. 10. Planetary wave amplitude for the regression patterns at 50 and 700 hPa.

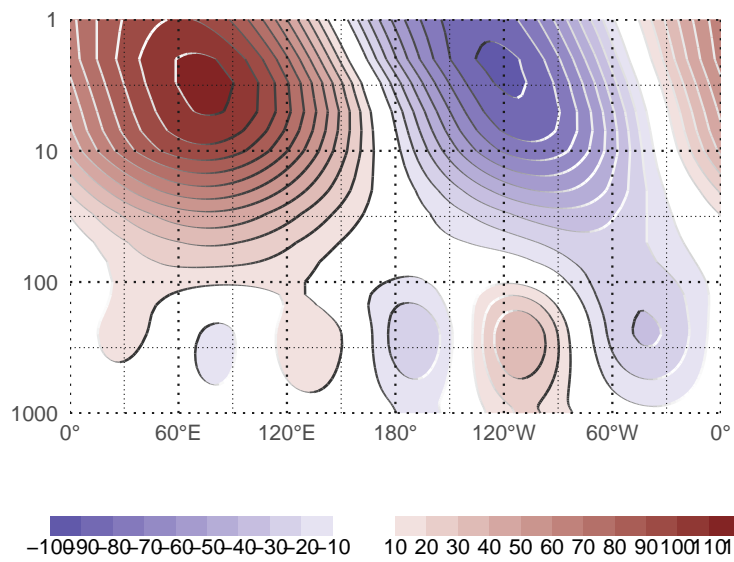


FIG. 11. Asymmetric coefficient of the multiple regression of mean monthly geopotential height anomalies
between 65 and 40 South. (this caption needs some love)

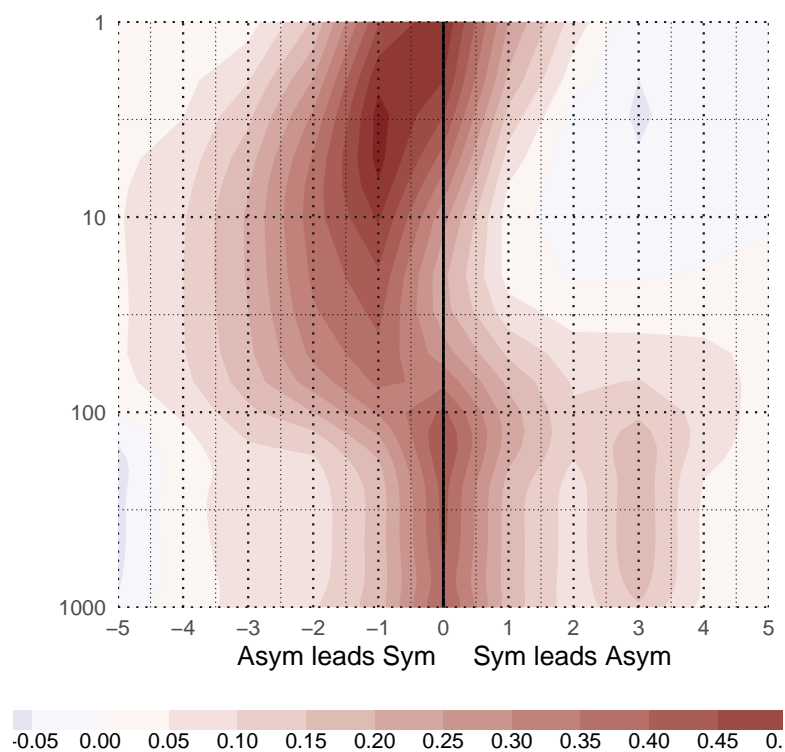


Fig. A1. Lag-correlation between Symmetric and Asymmetric SAM at each level.

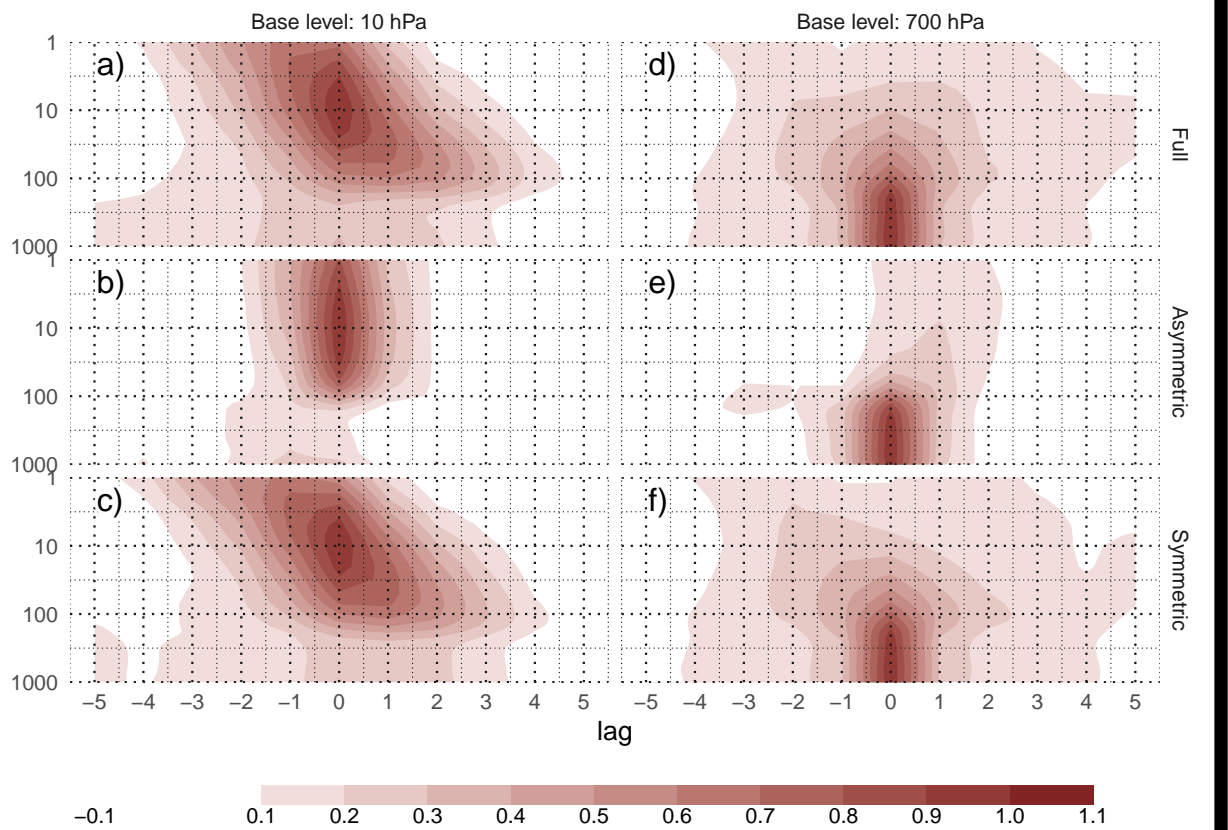


FIG. 12. Cross-correlation functions for each index and two different base levels.

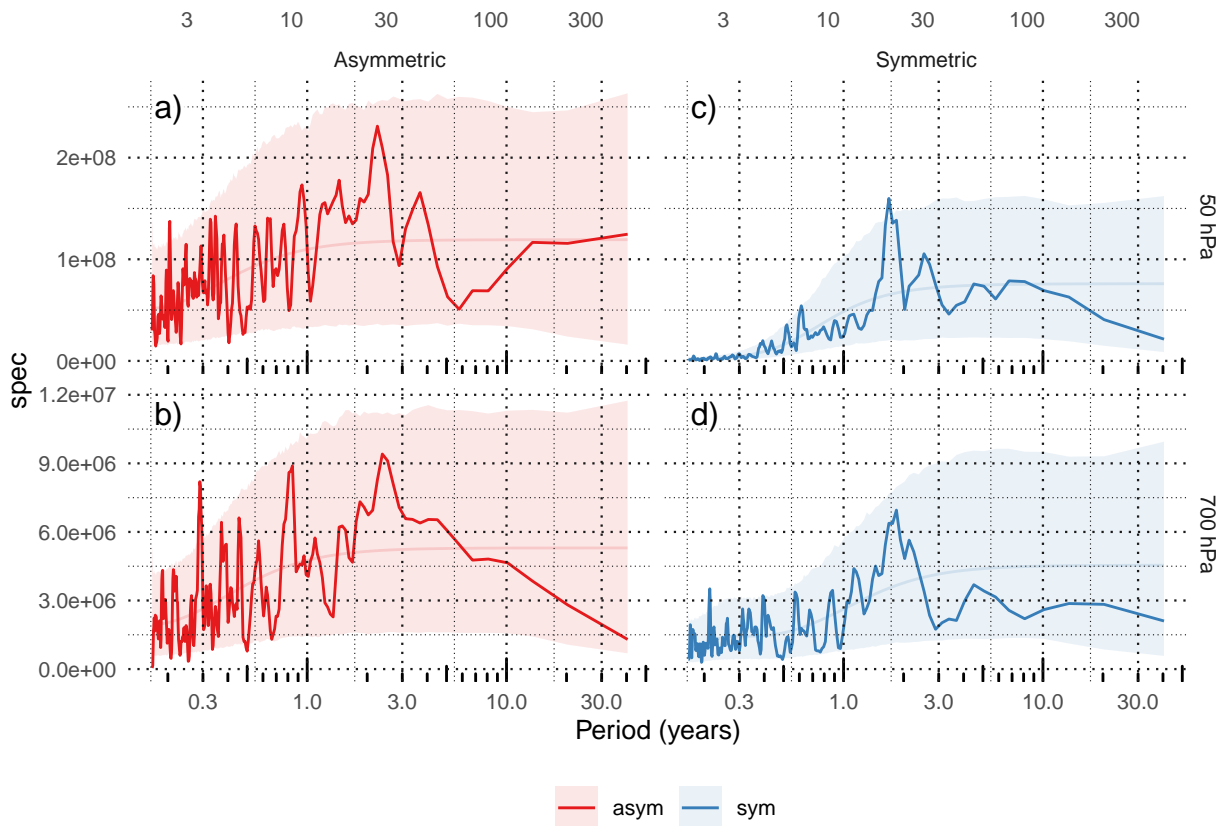


Fig. A2. Fourier spectrum of each timeseries. The shading indicates the 95% area derived by fitting an AR process to each series and bootstrapping 5000 simulated samples.

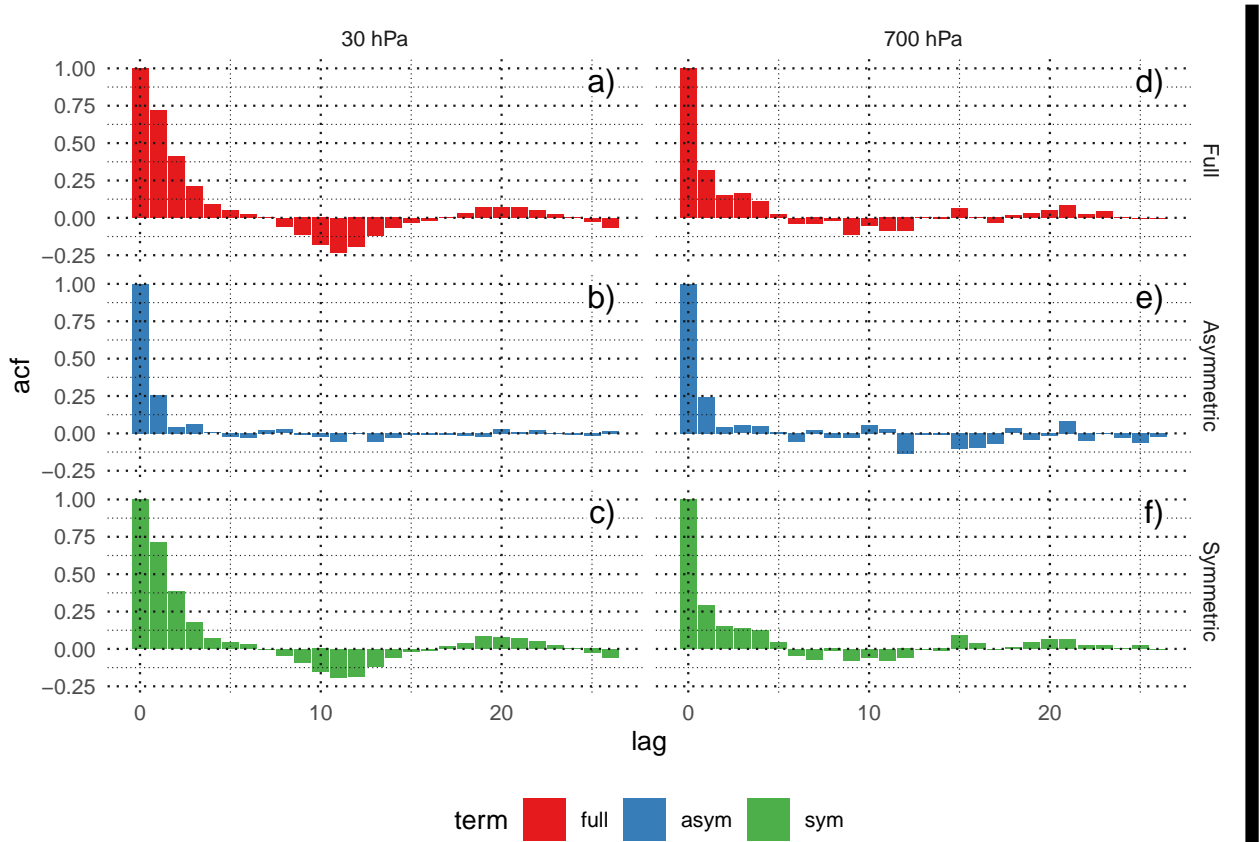


Fig. A3. Autocorrelation functions of each timeseries

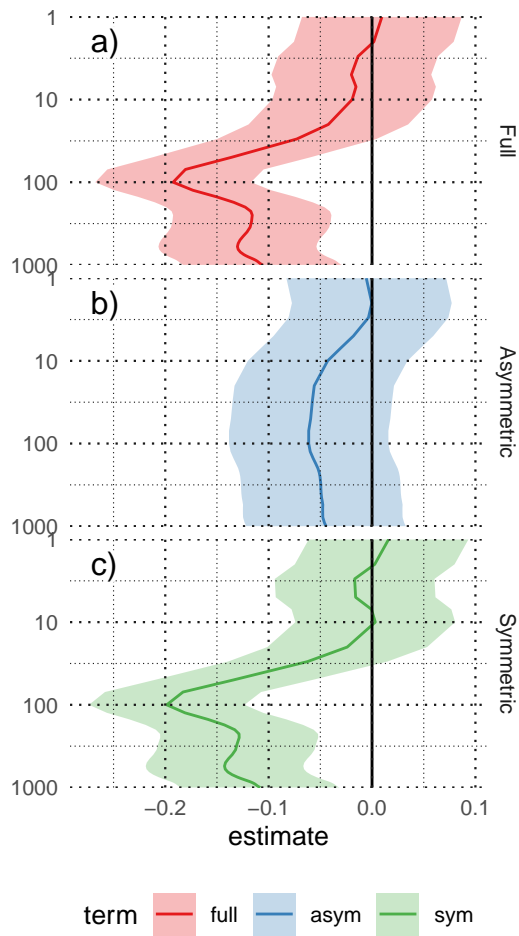


Fig. A4. Trends for each index at each level. Shading indicates the 95% confidence interval.

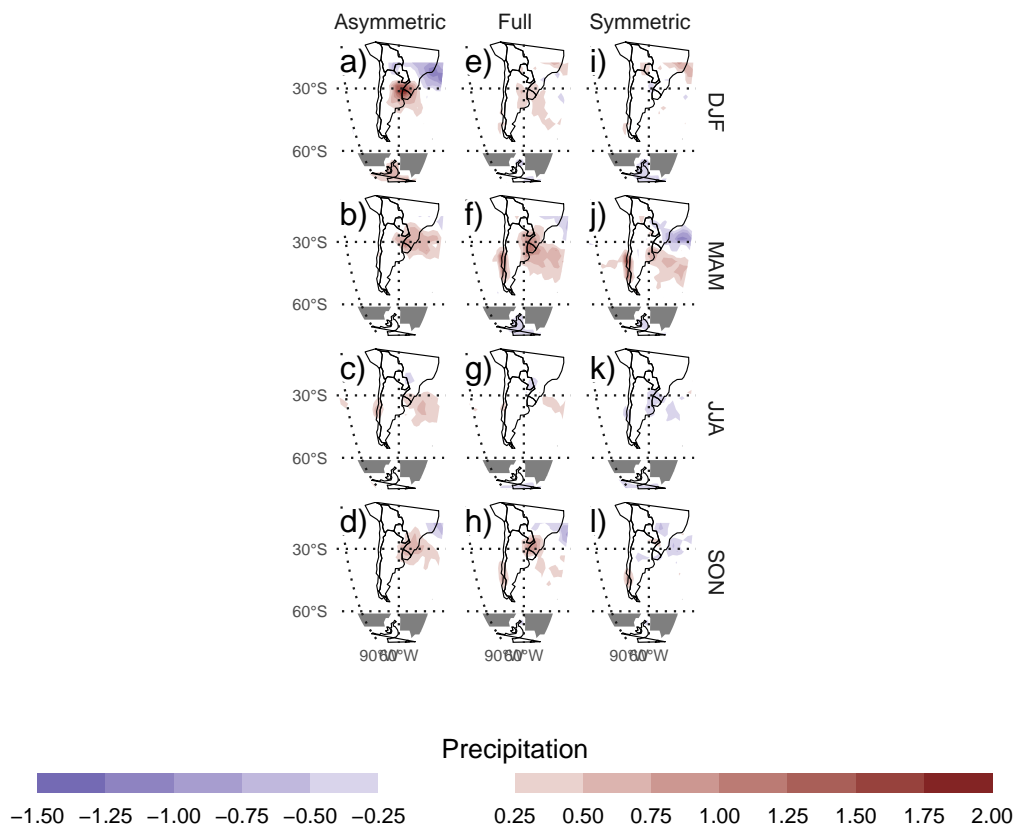
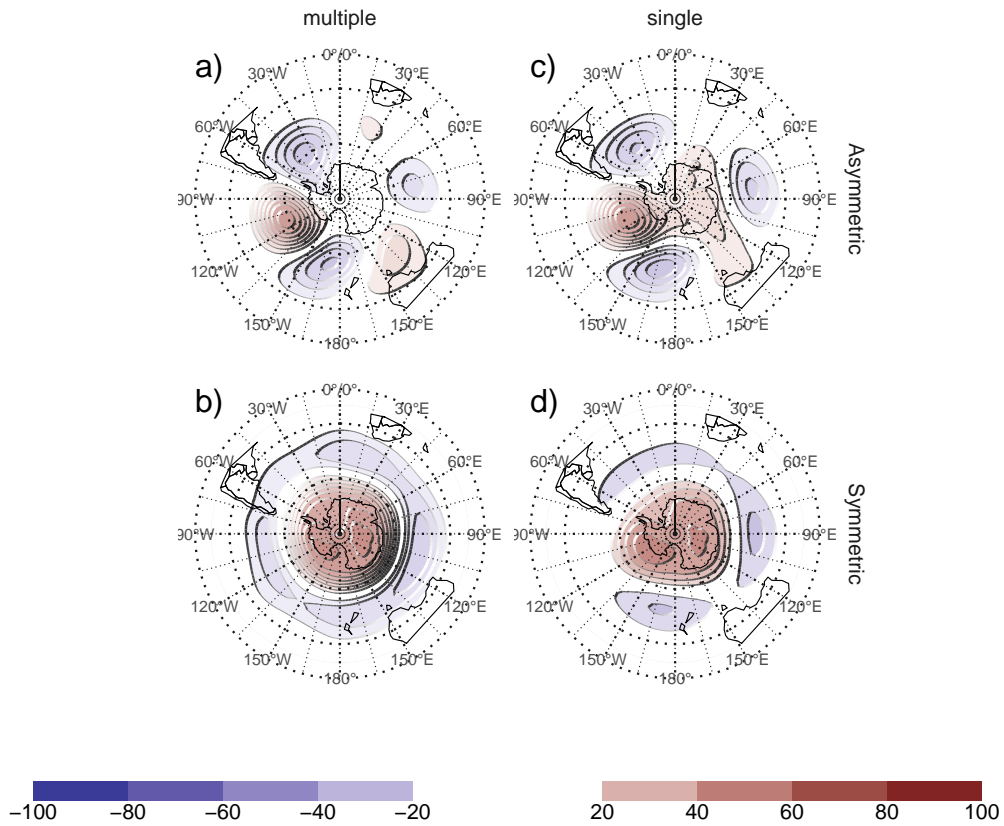


Fig. A5. Regression pattern of precipitation with Asymmetric and Symmetric SAM. P-values smaller than 0.05 (controlling for False Detection Rate) as hatched areas.



167 Fig. A6. Regressions maps resulting from performing one multiple regression (a. and b.) and from performing
 168 two simple regressions (c. and d.)

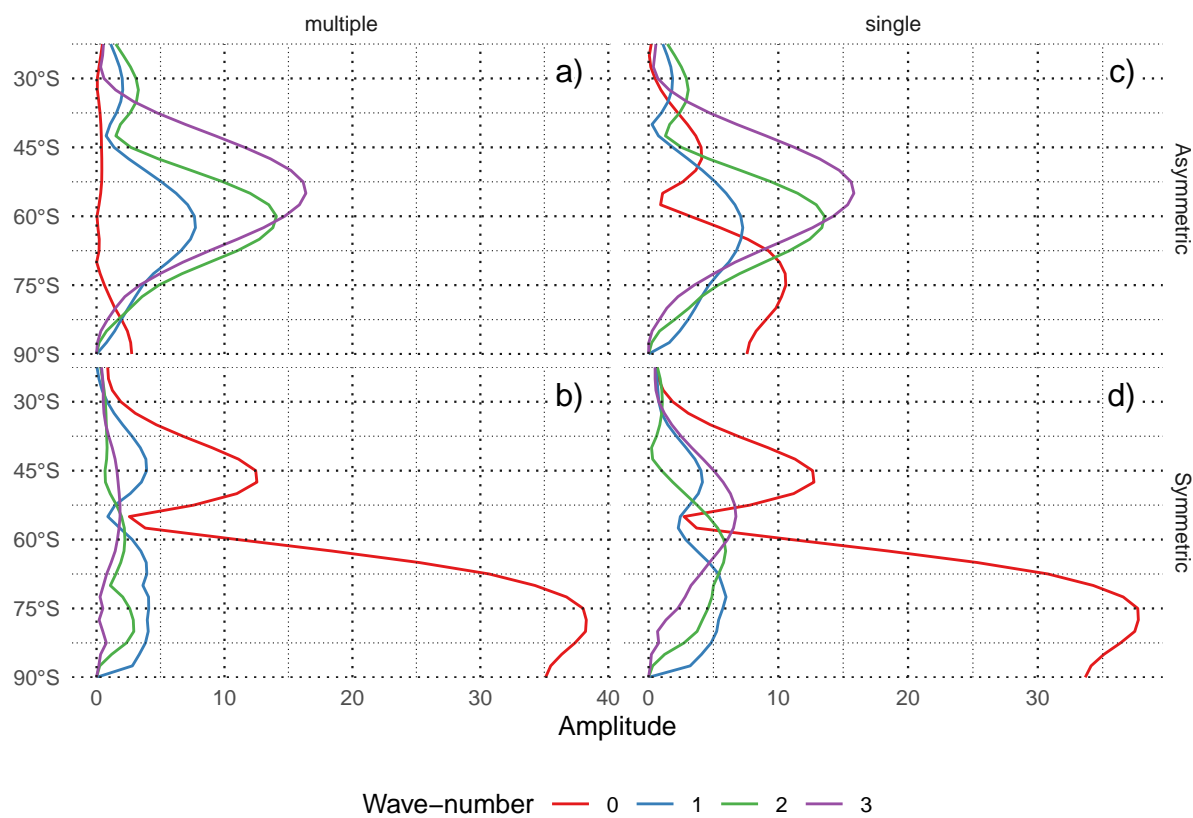


FIG. 13.